Preprint Title	Analysis of entropy generation with heat generation in time dependent hydromagnetic flow of nanofluid in an oscillatory semi-porous curved channel
Authors	Muhammad Imran, Zaheer Abbas and Muhammad Naveed
Publication Date	20 Oct 2021
Article Type	Full Research Paper
ORCID® iDs	Muhammad Imran - https://orcid.org/0000-0002-2760-3595; Muhammad Naveed - https://orcid.org/0000-0002-9616-3087

Analysis of entropy generation with heat generation in time dependent hydromagnetic flow of nanofluid in an oscillatory semi- porous curved channel

M. Imran[a], Z. Abbas[b], and M. Naveed[c,1]

[a]Government of Punjab School Education Department,
Rahim Yar Khan 64200, Pakistan
[b]Department of Mathematics, The Islamia University of Bahawalpur,
Bahawalpur 63100, Pakistan.
[c]Department of Mathematics, KhwajaFareed University of Engineering
& Information Technology Rahim Yar Khan 64200, Pakistan

Abstract: The present study focusses on the investigation of thermodynamic optimization of hydromagnetic time dependent boundary layer nanofluid flow by employing entropy generation method (EMG) in semi- permeable oscillatory curved channel. We used Buongiorno model for nanofluid to address the impact of the parameters of Brownian motion and thermophoresis. The consequences of heat production are also taken into consideration in energy the equation. The mathematical form of boundary layer equations is accomplished by following the curvilinear coordinates scheme for the considered flow problem. The analytical convergent solution of the determined nonlinear PDEs is achieved through the process of homotopy analysis (HAM). A detailed analysis is conducted out to analyze the consequences of dissimilar variables concerned, such as non-dimensional radius of curvature, Lewis number, magnetic parameter, relation of wall oscillation frequency to its parameter of velocity, Reynolds number, Prandtl number, heat production and thermophoresis parameters, entropy generation rate, Brownian motion parameter and Brickman number, concentration and temperature difference parameters on temperature, velocity profile, concentration, pressure, drag surface force, Bejan number, entropy generation, rate of mass and heat transport are addressed in detail via tables and graphs. It is noted that, the magnitude of heat transmission rate (local Nusselt number) steadily decays for advanced values of radius of curvature variable and Reynolds number.

Keywords: Semi-porous curved oscillatory channel, viscous nanofluid, entropy generation, heat generation, magnetohydrodynamic (MHD), Homotopy analysis method.

1. Introduction

The analysis of various fluid dynamics in tubes or semi-porous/ porous channels has obtained a lot of attention from many scientists and researchers over the last few decades owing to its

---

[1]Corresponding Author. Tel.: +92 62 9255480

e-mail address: rana.m.naveed@gmail.com (M. Naveed)

broad range of practical applications in mechanical and biomedical engineering. Such applications includes permeable or semi-permeable pipes processing, movement of blood in oxygenators, capillary blood flow, filters design and blood dialysis in synthetic kidney. Berman [1] initiated the first research on steady flow phenomenon of viscous fluid in porous channel. He provided an exact solution to the acquired Navier stokes equations. After Berman [1], both for viscous and non-Newtonian liquids, several researchers extended his concept in different directions. White [2] examined incompressible viscous fluid flow via an uniformly permeable channel. Abbas et al. [3] conducted a analytical study for the hydromagnetic boundary layer Maxwell fluid flow inside a porous channel. Raftari and Vajravelu [4] has computed analytical results for hydromagnetic viscoelastic liquid flow and heat transfer in a stretchable wall channel by means of homotopy analysis method. Ali et al. [5] performed an analysis of the hydromagnetic Oldroyd-B liquid flow and heat transport inside a channel. Abbas et al. [6] performed an analytical examination of Maxwell liquid motion in an axis-symmetric semi-permeable channel by incorporating perturbation approach. Heat transfer research for channel flow of MHD Jeffery liquid with generalized boundary conditions was reported by Aleem et al. [7].

The examination of flow through some kind of narrow, curved type channel has acquired high significance as a result of its multiple physical applications in many biomedical and industrial processes. Khuri [8] conducted a study for the Stokes motion in a curved channel. The impacts of forced convection and porosity on curved reciprocating channel flow were tested by Fu et al. [9]. Abbas et al. [10] proposed a numerical study for nonlinear transfer of thermal energy with Hall impacts in flow of viscous liquid inside a curved semi- permeable channel. Naveed et al. [11] examine the impact of thermal radiation and permeability material on motion of flowing liquid via a curved semi- porous channel. Sajid et al. [12] has computed joule heating impacts on magnetic nanoparticles through a semi-porous curved channel. The impacts of the applied constant magnetic field on the thermally heated flow of Carreau liquid within a curved channel was evaluated by Abbas et al. [13]. Numerical outcomes for heat transfer process in Powell-Eyring liquid flow through a curved channel with Cattaneo-Christov heat flux model was computed by Abbas et al. [14].

The research of oscillatory flows is a fundamental theory in the field of biological and engineering processes such as oil drilling, blood flow control during surgical treatment, oil exploration, lungs respiratory functions processing, manufacturing and processing of foods and papers, cosmetic products, chemical /blood dispensing modeling in biochemistry /clinical laboratories etc. Misra et al. [15] evaluated the heat transfer in viscoelastic hydromagnetic fluid flow in a stretchable wall oscillating channel. Ali et al. [16] examined time dependent oscillatory flow of viscoelastic fluid in a permeable channel with heat and mass transfer. Ali and Asghar [17] conducted analytical solution for Jeffery fluid flow in an oscillatory channel. Khan et al. [18] investigated the heat transfer characteristics in hydromagnetic Maxwell fluid flow within an oscillatory channel with Cattaneo- Christov heat model. Abbas et al. [19] detected the influences of linear thermal radiation in time dependent motion of flowing liquid across a convectively heated curved oscillating stretchable surface. Very recently, Imran et al.

[20] evaluated the impacts of applied magnetic field and heat production in flow of ferrofluid past over a curved stretching oscillatory sheet.

The analysis of heat transfer in flow of nanofluids has attained considerable attention by the researchers due to its numerous utilizations in the fields, like space cooling, microelectronic cooling and modern generation of cooling technology. Fluids such as ethylene glycol, oil and water are examples of base fluids having low thermal conductivity. With the addition of certain nano-sized particles (less than 1%), the thermal conductivity of such base fluids can be improved and they form nanofluids. Choi [21] initially presented the idea of nanofluids. After that, by considering the impacts of thermophoresis and the Brownian motion of the nanoparticles, Buongiorno [22] introduced a new definition of nanofluids. Sheikoleslami et al. [23] addressed the analytical outcomes for MHD flow of nanofluid in a semi-porous channel. Naveed et al. [24] deliberated the consequences of Brownian motion and thermophoretic in the existence of thermal radiation for the Blasius motion of nanoliquid across a curved stretchable sheet. Alblawi et al. [25] has detected Buongiorno's nanoliquid model across a curved exponentially stretchable wall. Rashed and Ahmed [26] has investigated peristaltic flow of dusty nanofluids inside curved channel. Riaz et al. [27] investigated the heat transfer mechanism in peristaltic flow of nanoparticles through a curved channel with second order slip condition.

The main purpose of the present study is to examine the entropy production rate in presence of applied magnetic field on time dependent flow of nanofluid in a semi-porous oscillatory curved channel. The implications of heat production are also included in heat equation. The governing partial differential equations describing the flow phenomenon are highly complex and nonlinear in nature which is solved analytically by utilizing an efficient analytical technique called homotopy analysis method. The description of this article is as follows: Section 2 gives the mathematical development of the flow problem with appropriate boundary conditions; Section 3 gives the rate of entropy generation on the flow; Section 4 is all about analytical simulation in series form; Section 5 comprises of discussion of obtained results and Section 6 summarizes some concluding remarks.

2. Mathematical development

Consider hydromagnetic time dependent and boundary layer two dimensional motion of an incompressible nanoliquid inside the walls of curved semi-permeable channel that are separated by distance $\bar{H}$ coiled in a semi-circle of radius $\bar{A}$. The viscous fluid is injected through upper wall of the channel which is considered porous and lower wall is considered oscillatory. The lower oscillatory wall having temperature $\bar{T}_w$ moves continually to and fro about origin with periodic velocity $\bar{w} = \bar{U}_w \sin \bar{\omega} \bar{t}$. Here $\bar{U}_w$ and $\bar{\omega}$ are considered velocity and oscillatory frequency of the wall respectively. Let $\bar{T}_1$ be the temperature of the upper wall with $\bar{T}_w > \bar{T}_1$. Also let $\bar{C}_w$ and $\bar{C}_1$ be the concentrations at lower and at upper permeable

walls with $\bar{C}_w > \bar{C}_1$. In radial $\bar{x}$ direction, a constant magnetic field of strength B_0 is imposed. The boundary layer equations for the flow problem under considerations are
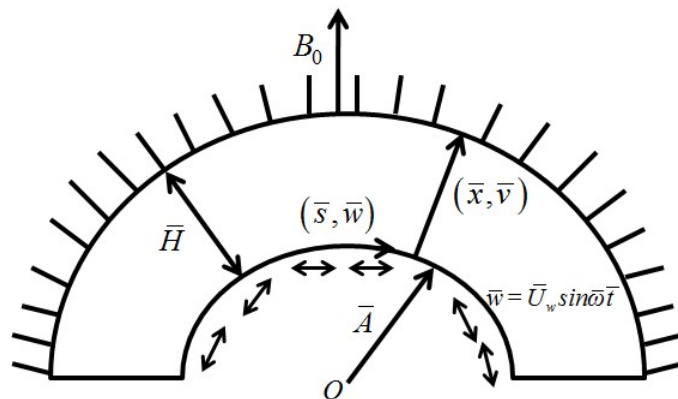
Fig.1. Schematic flow geometry

$$\frac{\partial \bar{w}}{\partial \bar{s}} \bar{A} + \frac{\partial}{\partial \bar{x}}\left\{ \left(\bar{A} + \bar{x}\right)\bar{v}\right\} = 0,$$ (1)

$$\frac{1}{\bar{\rho}} \frac{\partial \bar{p}}{\partial \bar{x}} = \frac{\bar{w}^2}{\bar{x} + \bar{A}},$$ (2)

$$\frac{\partial \bar{w}}{\partial \bar{t}} + \frac{\partial \bar{w}}{\partial \bar{x}}\bar{v} + \frac{\bar{A}\bar{w}}{\bar{A}+\bar{x}}\frac{\partial \bar{w}}{\partial \bar{s}} + \frac{\bar{w}\bar{v}}{\bar{A}+\bar{x}} = -\frac{1}{\bar{\rho}}\frac{\bar{A}}{\bar{A}+\bar{x}}\frac{\partial \bar{p}}{\partial \bar{s}}$$

$$+\bar{v}\left(\frac{\partial^2 \bar{w}}{\partial \bar{x}^2} - \frac{\bar{w}}{\left(\bar{A}+\bar{x}\right)^2} + \frac{1}{\bar{A}+\bar{x}}\frac{\partial \bar{w}}{\partial \bar{r}}\right) - \frac{\bar{\sigma}}{\bar{\rho}}B_0^2 \bar{w},$$ (3)

$$\frac{\partial \bar{T}}{\partial \bar{t}} + \frac{\bar{A}\bar{w}}{\bar{A}+\bar{x}}\frac{\partial \bar{T}}{\partial \bar{s}} + \frac{\partial \bar{T}}{\partial \bar{x}}\bar{v} = \bar{\alpha}\left(\frac{\partial^2 \bar{T}}{\partial \bar{x}^2} + \frac{1}{\bar{A}+\bar{x}}\frac{\partial \bar{T}}{\partial \bar{x}}\right)$$

$$+\bar{\tau}_\alpha \left(\bar{D}_B \left(\frac{\partial \bar{C}}{\partial \bar{x}}\frac{\partial \bar{T}}{\partial \bar{x}}\right) + \frac{\bar{D}_T}{\bar{T}_0}\left(\frac{\partial \bar{T}}{\partial \bar{x}}\right)^2 \right) + \frac{\bar{Q}}{\left(\bar{\rho}\bar{c}\right)_{\bar{f}}}\left(\bar{T} - \bar{T}_0\right),$$ (4)

$$\frac{\partial \bar{C}}{\partial \bar{t}} + \frac{\bar{A}\bar{w}}{\left(\bar{A}+\bar{x}\right)}\frac{\partial \bar{C}}{\partial \bar{s}} + \frac{\partial \bar{C}}{\partial \bar{x}}\bar{v} = \bar{D}_B \left(\frac{\partial^2 \bar{C}}{\partial \bar{x}^2} + \frac{1}{\left(\bar{A}+\bar{x}\right)}\frac{\partial \bar{C}}{\partial \bar{x}}\right)$$

$$+\frac{\bar{D}_T}{\bar{T}_1}\left(\frac{\partial^2 \bar{T}}{\partial \bar{x}^2} + \frac{1}{\left(\bar{A}+\bar{x}\right)}\frac{\partial \bar{T}}{\partial \bar{x}}\right),$$ (5)

In overhead equations, $\bar{w}$ and $\bar{v}$ are considered to be the velocity parts along $\bar{s}$ and $\bar{x}$ – directions, $\bar{\rho}$ the density, $\bar{p}$ the pressure, $\bar{D}_T$ indicates the thermophoretic diffusion, $\bar{\alpha} = \bar{k}_{\bar{\alpha}} / \left(\bar{c}_{\bar{f}}\bar{\rho}_{\bar{f}}\right)$ represents the thermal diffusivity, $\bar{c}_{\bar{p}}$ the specific heat capacity at uniform

4

pressure, $\bar{D}_B$ representing the coefficient of Brownian diffusion, $\bar{v}$ the kinematic viscosity, $\bar{\tau}_\alpha = \left(\bar{c}_{\bar{p}} \bar{\rho}_{\bar{p}} \right) / \left(\bar{\rho}_{\bar{f}} \bar{c}_{\bar{f}} \right)$ relation of the heat capability to the material ration of the fluid, $\bar{C}$ the concentration and $\bar{T}$ the temperature of the fluid.

The boundary conditions related with the existing motion problem are

$$\left.\begin{array}{l} \bar{T} = \bar{T}_w, \ \ \bar{w} = \bar{U}_w \sin \bar{\omega} \bar{t}, \ \ \bar{C} = \bar{C}_w, \ \ \bar{v} = 0, \ \ \text{at } \bar{x} = 0, \\[2mm] \bar{T} \to \bar{T}_1, \ \ \bar{u} = 0, \ \ \bar{v} = \dfrac{-\bar{U}_w \bar{A}}{\bar{A} + \bar{x}}, \ \ \bar{C} \to \bar{C}_1, \ \ \text{as } \bar{x} = \bar{H}. \end{array}\right\} \tag{6}$$

Where $\bar{U}_w < 0$ denotes injection and $\bar{U}_w > 0$ denote the suction velocity respectively.

We will now initiate the following non-dimensional variables as

$$\begin{array}{l} \dfrac{\bar{x}}{\bar{H}} = \bar{\xi}, \ \ \bar{f}_{\bar{\xi}}(\bar{\xi}, \bar{\tau}) \bar{U}_w = \bar{w}, \ \ \bar{t} \bar{\omega} = \bar{\tau}, \ \ \dfrac{-\bar{A} \bar{U}_w}{\bar{A} + \bar{x}} \bar{f}(\bar{\xi}, \bar{\tau}) = \bar{v}, \\[3mm] \dfrac{\bar{\rho} \bar{U}_w^2 \bar{s}^2}{\bar{H}^2} \bar{P}(\bar{\xi}, \bar{\tau}) = \bar{p}, \ \ \bar{T} - \bar{T}_1 = \left(\bar{T}_w - \bar{T}_1 \right) \bar{\theta}(\bar{\xi}, \bar{\tau}), \\[3mm] \bar{C} - \bar{C}_1 = \left(\bar{C}_w - \bar{C}_1 \right) \bar{\phi}(\bar{\xi}, \bar{\tau}) \end{array} \tag{7}$$

Via the application of Eq. (7) Eq. (1) is verified on identical basis, and remaining Eqs. (2- 5) yields

$$\bar{P}_{\bar{\xi}} = \frac{1}{\left(C_1 + \bar{\xi} \right)} \bar{f}_{\bar{\xi}}^{\,2}, \tag{8}$$

$$\bar{P}(\bar{\xi}, \bar{\tau}) = \frac{C_1 + \bar{\xi}}{2 C_1 Re} \left(\begin{array}{l} \bar{f}_{\bar{\xi}\bar{\xi}\bar{\xi}} + \dfrac{\bar{f}_{\bar{\xi}\bar{\xi}}}{\left(\bar{\xi} + C_1 \right)} - \dfrac{\bar{f}_{\bar{\xi}}}{\left(\bar{\xi} + C_1 \right)^2} - M^2 \bar{f}_{\bar{\xi}} - S \bar{f}_{\bar{\xi}\bar{\tau}} \\[3mm] - \bar{f}_{\bar{\xi}}^{2} \dfrac{C_1}{\left(\bar{\xi} + C_1 \right)} + \dfrac{C_1}{\left(\bar{\xi} + C_1 \right)} \bar{f} \, \bar{f}_{\bar{\xi}\bar{\xi}} + \bar{f} \, \bar{f}_{\bar{\xi}} \dfrac{C_1}{\left(\bar{\xi} + C_1 \right)^2} \end{array} \right), \tag{9}$$

$$\frac{1}{Pr} \left(\bar{\theta}_{\bar{\xi}\bar{\xi}} + \frac{\bar{\theta}_{\bar{\xi}}}{\left(\bar{\xi} + C_1 \right)} \right) + Re \left(\frac{C_1}{\left(\bar{\xi} + C_1 \right)} \bar{f} \bar{\theta}_{\bar{\xi}} - S \bar{\theta}_{\bar{\tau}} + \lambda \bar{\theta} \right) + \left(\begin{array}{l} Nt \bar{\theta}_{\bar{\xi}}^{2} \\ + Nb \bar{\theta}_{\bar{\xi}} \bar{\phi}_{\bar{\xi}} \end{array} \right) = 0, \tag{10}$$

$$\frac{1}{Le} \left(\bar{\phi}_{\bar{\xi}\bar{\xi}} + \frac{\bar{\phi}_{\bar{\xi}}}{\left(\bar{\xi} + C_1 \right)} \right) + Re \left(\frac{C_1}{\left(\bar{\xi} + C_1 \right)} \bar{f} \bar{\phi}_{\bar{\xi}} - S \bar{\phi}_{\bar{\tau}} \right) + \frac{Nt}{Le Nb} \left(\bar{\theta}_{\bar{\xi}\bar{\xi}} + \frac{\bar{\theta}_{\bar{\xi}}}{\left(C_1 + \bar{\xi} \right)} \right) = 0, \tag{11}$$

where, $C_1 \left(= \bar{A} / \bar{H} \right)$ implies the non- dimensional term of the radius of curvature, $Nt \left(= \bar{\tau}_\alpha \bar{D}_T \left(\bar{T}_w - \bar{T}_1 \right) / \bar{v} \bar{T}_1 \right)$ the thermophoresis parameter, $S \left(= \bar{H} \bar{\omega} / \bar{U}_w \right)$ the relation of the wall oscillation frequency to the wall velocity, $Pr \left(= \bar{v} / \bar{\alpha} \right)$ the Prandtl number, $Re \left(= \bar{H} \bar{U}_w / \bar{v} \right)$ the

Reynolds number , $Le\left(=\bar{v}/\bar{D}_B\right)$ the Lewis number, $M^2\left(=\bar{\sigma}B_0^2\bar{H}/\bar{\rho}\bar{U}_w\right)$ the magnetic parameter, $\lambda\left(=\bar{H}\bar{Q}/\bar{U}_w\left(\bar{c}\bar{\rho}\right)_{\bar{f}}\right)$ the heat production parameter and $Nb\left(=\bar{\tau}_\alpha\bar{D}_B\left(\bar{C}_w-\bar{C}_1\right)/\bar{v}\right)$ represents the parameter of Brownian motion respectively.

After removing the term of pressure from the Eqs. (8) and (9), the liquid velocity can be accomplished as

$$\bar{f}_{\bar{\xi}\bar{\xi}\bar{\xi}\bar{\xi}}+\frac{2\bar{f}_{\bar{\xi}\bar{\xi}\bar{\xi}}}{\left(C_1+\bar{\xi}\right)}-\frac{\bar{f}_{\bar{\xi}\bar{\xi}}}{\left(C_1+\bar{\xi}\right)^2}+\frac{\bar{f}_{\bar{\xi}}}{\left(C_1+\bar{\xi}\right)^3}-\left(\bar{f}_{\bar{\xi}\bar{\xi}\bar{\tau}}+\frac{\bar{f}_{\bar{\xi}\bar{\tau}}}{C_1+\bar{\xi}}\right)SRe$$

$$-\frac{ReC_1}{\left(C_1+\bar{\xi}\right)}\left(\bar{f}_{\bar{\xi}}\bar{f}_{\bar{\xi}\bar{\xi}}-\bar{f}_{\bar{\xi}\bar{\xi}\bar{\xi}}\bar{f}\right)-\frac{C_1Re}{\left(C_1+\bar{\xi}\right)^2}\left(\bar{f}_{\bar{\xi}}^2-\bar{f}_{\bar{\xi}\bar{\xi}}\bar{f}\right) \qquad (12)$$

$$-\left(\bar{f}_{\bar{\xi}\bar{\xi}}+\frac{\bar{f}_{\bar{\xi}}}{C_1+\bar{\xi}}\right)M^2Re-\frac{C_1Re}{\left(C_1+\bar{\xi}\right)^3}\bar{f}_{\bar{\xi}}\bar{f}=0.$$

With following boundary conditions

$$\bar{\theta}\left(0,\bar{\tau}\right)=1,\ \bar{f}_{\bar{\xi}}\left(0,\bar{\tau}\right)=sin\bar{\tau},\ \bar{\phi}\left(0,\bar{\tau}\right)=1,\ \bar{f}\left(0,\bar{\tau}\right)=0,$$

$$\bar{f}_{\bar{\xi}}\left(1,\bar{\tau}\right)=\bar{\theta}\left(1,\bar{\tau}\right)=\bar{\phi}\left(1,\bar{\tau}\right)=0,\ \bar{f}\left(1,\bar{\tau}\right)=1. \qquad (13)$$

The drag surface force, the transmission heat and mass rate along the curved wall is characterized as

$$\bar{C}_{\bar{f}}=\frac{\tau_{\bar{r}\bar{s}}}{\bar{\rho}\bar{u}_w^2},\qquad \bar{N}\bar{u}_{\bar{s}}=\frac{\bar{s}\,\bar{q}_{\bar{w}}}{\left(\bar{T}_w-\bar{T}_1\right)\bar{k}_\alpha},\qquad \bar{S}\bar{h}_{\bar{s}}=\frac{\bar{s}\,\bar{j}_{\bar{w}}}{\left(\bar{C}_w-\bar{C}_1\right)\bar{D}_B} \qquad (14)$$

here, $\tau_{\bar{r}\bar{s}}$, $\bar{q}_{\bar{w}}$ and $\bar{j}_{\bar{w}}$ are depicted by

$$\tau_{\bar{r}\bar{s}}=\bar{\mu}\left(\frac{\partial\bar{w}}{\partial\bar{x}}-\frac{\bar{w}}{\bar{A}+\bar{x}}\right)\Bigg|_{\bar{x}=0},\quad \bar{q}_{\bar{w}}=-\left(\bar{k}_\alpha\frac{\partial\bar{T}}{\partial\bar{x}}\right)\Bigg|_{\bar{x}=0},\quad \bar{j}_{\bar{w}}=-\left(\bar{D}_B\frac{\partial\bar{C}}{\partial\bar{x}}\right)\Bigg|_{\bar{x}=0} \qquad (15)$$

Making apply of Eq. (7) in Eqs. (14) and (15), we attain

$$Re_{\bar{s}}^{1/2}\bar{C}_{\bar{f}}=\frac{1}{C_1}\left[C_1\bar{f}_{\bar{\xi}\bar{\xi}}\left(0,\bar{\tau}\right)-\bar{f}_{\bar{\xi}}\left(0,\bar{\tau}\right)\right], \qquad (16)$$

$$Re_{\bar{s}}^{-1/2}\bar{N}\bar{u}_{\bar{s}}=-\bar{\theta}_{\bar{\xi}}\left(0,\bar{\tau}\right), \qquad (17)$$

$$Re_{\bar{s}}^{-1/2}\bar{S}\bar{h}_{\bar{s}}=-\bar{\phi}_{\bar{\xi}}\left(0,\bar{\tau}\right). \qquad (18)$$

here, $Re_{\bar{s}}^{1/2}=\bar{U}_w\bar{s}/\bar{v}$ represents the Reynolds number.

3. Entropy Generation

The velocity of the liquid, concentration and temperature fields once accomplished can be used for the calculation of the entropy production rate in an oscillatory curved porous channel. Entropy production depicts the irreversible action of the mechanism induced by heat flow, electric conduction of nanofluid and fluid friction. Entropy production rate in dimensional form for magnetohydrodynamic flow of nanofluid inside an oscillatory curved semi-porous channel can expressed as

$$\bar{S}_{\bar{E}} = \underbrace{\frac{\bar{k}_{\bar{\alpha}}}{\bar{T}_1^2}\left(\frac{\partial \bar{T}}{\partial \bar{x}}\right)^2}_{\text{Thermal irreversibility}} + \underbrace{\frac{\bar{\mu}}{\bar{T}_1}\left(\frac{\partial \bar{w}}{\partial \bar{x}} + \frac{\bar{w}}{\left(\bar{A}+\bar{x}\right)}\right)^2}_{\text{Fluid Friction irreversibility}}$$
$$+ \underbrace{\frac{\bar{\sigma}\bar{B}_0^2\bar{w}^2}{\bar{T}_1}}_{\text{Joule Heating irreversibility}} + \underbrace{\frac{\bar{D}_B}{\bar{T}_1}\left(\frac{\partial \bar{T}}{\partial \bar{x}}\frac{\partial \bar{C}}{\partial \bar{x}}\right) + \frac{\bar{D}_B}{\bar{C}_1}\left(\frac{\partial \bar{C}}{\partial \bar{x}}\right)^2}_{\text{Concentration irreversibility}}, \tag{19}$$

Applying Eq. (7), the non-dimensional form of Eq. (19) is

$$\bar{N}_{\bar{G}} = \frac{\delta_1\alpha_2}{\alpha_1}\bar{\phi}_{\bar{\xi}}^2 + \alpha_1\bar{\theta}_{\bar{\xi}}^2 + \delta_1\bar{\theta}_{\bar{\xi}}\bar{\phi}_{\bar{\xi}} + Br\left(\bar{f}_{\bar{\xi}\bar{\xi}} + \frac{\bar{f}_{\bar{\xi}}}{\left(C_1+\bar{\xi}\right)}\right)^2 + M^2BrRe\bar{f}_{\bar{\xi}}^2, \tag{20}$$

Where, $\bar{N}_{\bar{G}}\left(=\bar{H}^2\bar{T}_1\bar{S}_{\bar{E}}/\bar{k}_{\bar{\alpha}}\left(\bar{T}_w-\bar{T}_1\right)\right)$ represents the entropy production rate, $\alpha_2\left(=\left(\bar{C}_w-\bar{C}_1\right)/\bar{C}_1\right)$ the concentration difference parameter, $\alpha_1\left(=\left(\bar{T}_w-\bar{T}_1\right)/\bar{T}_1\right)$ the temperature difference parameter, $\delta_1\left(=\bar{D}_B\left(\bar{C}_w-\bar{C}_1\right)/\bar{k}_{\bar{\alpha}}\right)$ the dimensionless diffusion parameter and $Br\left(=\bar{\mu}\bar{U}_w^2\bar{s}^2/\bar{H}^2\bar{k}_{\bar{\alpha}}\left(\bar{T}_w-\bar{T}_1\right)\right)$ the Brinkman number respectively.

The dimensionless Bejan number is defined as

$$\bar{Be} = \frac{\text{Heat transfer irreversibility} + \text{concentration irreversbility}}{\text{Total irreversibility}}, \tag{21}$$

$$\bar{Be} = \frac{\alpha_1\bar{\theta}_{\bar{\xi}}^2 + \delta_1\bar{\theta}_{\bar{\xi}}\bar{\phi}_{\bar{\xi}} + \dfrac{\delta_1\alpha_2}{\alpha_1}\bar{\phi}_{\bar{\xi}}^2}{\alpha_1\bar{\theta}_{\bar{\xi}}^2 + Br\left(\bar{f}_{\bar{\xi}\bar{\xi}} + \dfrac{\bar{f}_{\bar{\xi}}}{\left(K_1+\bar{\xi}\right)}\right)^2 + \delta_1\bar{\theta}_{\bar{\xi}}\bar{\phi}_{\bar{\xi}} + \dfrac{\delta_1\alpha_2}{\alpha_1}\bar{\phi}_{\bar{\xi}}^2 + M^2BrRe\bar{f}_{\bar{\xi}}^2}, \tag{22}$$

4. Solution methodology

The prime focus of this section is to briefly explain the method of homotopy analysis that we used to calculate the series solution of governing nonlinear PDEs (10- 12) with final boundary conditions (13). For this depiction, as initial assumption and linear auxiliary operators for concentration, temperature and velocity field we take the following expressions as

$$\overline{f}_0\left(\overline{\xi},\overline{\tau}\right)=\left(sin\overline{\tau}-2\right)\overline{\xi}^3-\left(2sin\overline{\tau}-3\right)\overline{\xi}^2+\left(sin\overline{\tau}\right)\overline{\xi}$$
$$\overline{\phi}_0\left(\overline{\xi},\overline{\tau}\right)=\left(1-\overline{\xi}\right),\ \overline{\theta}_0\left(\overline{\xi},\overline{\tau}\right)=\left(1-\overline{\xi}\right).$$

(23)

$$\overline{\mathbb{N}}_{\overline{f}}\left(\overline{f}\right)=\overline{f}_{\overline{\xi}\overline{\xi}\overline{\xi}\overline{\xi}},\ \overline{\mathbb{N}}_{\overline{\theta}}\left(\overline{\theta}\right)=\overline{\theta}_{\overline{\xi}\overline{\xi}},$$
$$\overline{\mathbb{N}}_{\overline{\phi}}\left(\overline{\phi}\right)=\overline{\phi}_{\overline{\xi}\overline{\xi}}$$

(24)

with

$$\overline{\mathbb{N}}_{\overline{f}}\left[\overline{A}_4\overline{\xi}^3+\overline{A}_3\overline{\xi}^2+\overline{A}_2\overline{\xi}+\overline{A}_1\right]=0,$$
$$\overline{\mathbb{N}}_{\overline{\theta}}\left[\overline{A}_6\overline{\xi}+\overline{A}_5\right]=0,$$
$$\overline{\mathbb{N}}_{\overline{\phi}}\left[\overline{A}_8\overline{\xi}+\overline{A}_7\right]=0,$$

(25)

The General solution of the problem is of the form

$$\overline{f}_r^*\left(\overline{\xi},\overline{\tau}\right)=\hat{\overline{f}}_r\left(\overline{\xi},\overline{\tau}\right)+\overline{A}_1+\overline{A}_2\overline{\xi}+\overline{A}_3\overline{\xi}^2+\overline{A}_4\overline{\xi}^3,$$

(26)

$$\overline{\theta}_r^*\left(\overline{\xi},\overline{\tau}\right)=\hat{\overline{\theta}}_r\left(\overline{\xi},\overline{\tau}\right)+\overline{A}_5+\overline{A}_6\overline{\xi},$$

(27)

$$\overline{\phi}_r^*\left(\overline{\xi},\overline{\tau}\right)=\hat{\overline{\phi}}_r\left(\overline{\xi},\overline{\tau}\right)+\overline{A}_7+\overline{A}_8\overline{\xi},$$

(28)

where $\hat{\overline{f}}_s\left(\overline{\xi},\overline{\tau}\right),\hat{\overline{\theta}}_s\left(\overline{\xi},\overline{\tau}\right)$ and $\hat{\overline{\phi}}_s\left(\overline{\xi},\overline{\tau}\right)$ signify a particular solution. With the help of final boundary conditions, the constants $\overline{A}_i\left(i=1,2,3,4,5,6,7,8\right)$ are computed as follows:

$$\bar{A}_1 = -\hat{\bar{f}}_s(0,\bar{\tau}), \quad \bar{A}_2 = -\frac{\partial \hat{\bar{f}}_s(0,\bar{\tau})}{\partial \bar{\xi}},$$

$$\bar{A}_3 = \frac{2\partial \hat{\bar{f}}_s(0,\bar{\tau})}{\partial \bar{\xi}} + \frac{\partial \hat{\bar{f}}_s(1,\bar{\tau})}{\partial \bar{\xi}} + 3\hat{\bar{f}}_s(0,\bar{\tau}) - 3\hat{\bar{f}}_s(1,\bar{\tau}),$$

$$\bar{A}_4 = -\frac{\partial \hat{\bar{f}}_s(1,\bar{\tau})}{\partial \bar{\xi}} + 2\hat{\bar{f}}_s(1,\bar{\tau}) - \frac{\partial \hat{\bar{f}}_s(0,\bar{\tau})}{\partial \bar{\xi}} - 2\hat{\bar{f}}_s(0,\bar{\tau})$$

$$\bar{A}_5 = -\hat{\bar{\theta}}_s(0,\bar{\tau}), \quad \bar{A}_6 = \hat{\bar{\theta}}_s(0,\bar{\tau}) - \hat{\bar{\theta}}_s(1,\bar{\tau}), \tag{29}$$

$$\bar{A}_7 = -\hat{\bar{\phi}}_s(0,\bar{\tau}), \quad \bar{A}_8 = \hat{\bar{\phi}}_s(0,\bar{\tau}) - \hat{\bar{\phi}}_s(1,\bar{\tau}).$$

5. Results and discussion

In this section, we concentrate on briefly explaining the outcomes of various involved parameters including non-dimensional radius of curvature (C_1), thermophoresis parameter (Nt), relation of oscillatory wall frequency to the velocity of the wall (S), Lewis number (Le), Reynolds number (Re), heat generation parameter (λ), magnetic parameter (M), Brownian motion parameter (Nb), Prandtl number (Pr), temperature difference parameter (α_1), Brickman number (Br), diffusion parameter (δ_1) and concentration difference parameter (α_2) on velocity field, concentration distribution, pressure field, entropy production profile, temperature distribution, surface drag force, Bejan number, rate of transmission of heat and mass via tables and graphs.

Table.1. illustrates that the magnitude of absolute values of heat transfer rate $\left(\overline{Nu}_{\bar{s}} \mathrm{Re}_{\bar{s}}^{-1/2}\right)$ are reduces for improving values of $(C_1), (Pr), (Re), (Nt), (\lambda)$ and (Nb) at $\bar{\tau} = 0.5\pi$. Table.2. highlights that the magnitude of absolute values of mass transmission rate $\left(\overline{S}\,\overline{h}_{\bar{s}} \mathrm{Re}_{\bar{s}}^{-1/2}\right)$ grows with varying $(C_1), (Pr), (Nb), (Re), (Nt)$ and (Le) at $\bar{\tau} = 0.5\pi$.

Fig.2. (a-d) is made to illustrates the 3- dimensional observation of the physical response of the axial and normal velocity components $\overline{w}(\overline{x}, \overline{t})$ and $\overline{v}(\overline{x}, \overline{t})$. Figs 2 (a) and 2 (c) are drawn to depicts the behavior of fluid particles velocity over lower oscillatory wall by considering very small values of $\overline{x}$ i.e. $(\overline{x} \to 0)$. On the other hand, figures 2(b) and 2(d) are plotted to demonstrates the behavior of fluid particles velocity over upper permeable wall of the channel by considering $(\overline{r} = 1)$.

Fig.3. (a- c) and Fig.4 (a- c) represent that the stream lines of velocity components show symmetrical manner and deviates from origin for time interval $\bar{t} \in (-0.5\pi, 0.5\pi)$, and express oscillatory response for $\bar{t} \in (0, 10\pi)$ and $\bar{t} \in (0, 2\pi)$ respectively.

Fig.5. (a- d) gives the outcomes of dissimilar flow variables like $(C_1), (Re), (M)$ and (S) in time interval $\bar{\tau} \in (0, 10\pi)$ on $\bar{f}'(\bar{\xi}, \bar{\tau})$ for $\bar{\xi} = 0.1$ from the wall of the channel. It is apparent from figures 5(a-c) that by mounting values of $(C_1), (Re)$ and (M), the liquid velocity amplitude $\bar{f}'(\bar{\xi}, \bar{\tau})$ is reduced. Whereas, Fig. 5(d) depicts uphill manner with (S).

The consequences of $(C_1), (Re), (M)$ and (S) on $\bar{f}'(\bar{\xi}, \bar{\tau})$ at $\bar{\tau} = 0.5\pi$ are explained through Fig.6.(a- d). Figure 6(a) witnessed that with uplifting (C_1) the fluid profile $\bar{f}'(\bar{\xi}, \bar{\tau})$ initially grows, but after $(\bar{\xi} = 0.5)$ it depicts reducing behavior. However, figures 6. (b,c,d) portrayed that with enlarging value of $(S), (Re)$ and (M), the liquid velocity decreases near the oscillatory wall and exhibits opposite trend after $(\bar{\xi} = 0.5)$.

Fig.7. (a- d) demonstrates that $\bar{P}(\bar{\xi}, \bar{\tau})$ amplitude enhances with improving values of $(C_1), (Re)$ and (S) and reduces with (M) in time intervals $\bar{\tau} \in (0, 10\pi)$. Fig.8. (a- d) gives the alteration in $\bar{P}(\bar{\xi}, \bar{\tau})$ at $\bar{\tau} = 0.5\pi$. Figs 8 (a) and 8(c) confirmed that $\bar{P}(\bar{\xi}, \bar{\tau})$ is diminishing function of (C_1) and (Re). While, figures 8(b, d) witnessed that with enlarging values of (M) and (S), the pressure distribution firstly declares improving demeanor and then finally reduces.

Figure.9. (a-d) detects that the liquid temperature distribution $\bar{\theta}(\bar{\xi}, \bar{\tau})$ increases with superior values of $(C_1), (Nt), (\lambda), (Pr)$ and (Nb), and it decays with altering values of Reynolds number (Re).

Fig.10. (a- d) presents the impacts of unalike variables $(C_1), (Nb), (Pr), (Re), (Nt)$ and (Le) at $\bar{\tau} = 0.5\pi$ on $\bar{\phi}(\bar{\xi}, \bar{\tau})$. It is clearly apparent that $\bar{\phi}(\bar{\xi}, \bar{\tau})$ declines gradually for all variables.

The alteration in entropy production field $\bar{N}_{\bar{G}}(\bar{\xi}, \bar{\tau})$ at $\bar{\tau} = 0.5\pi$ is explored through Fig.11. (a-d). Figures 11(a) and 11(c) clarifies that $\bar{N}_{\bar{G}}(\bar{\xi}, \bar{\tau})$ show increasing response with $(Br), (\alpha_1), (Nt)$ and (Nb). While figures 11(b,d) illustrates that the profile $\bar{N}_{\bar{G}}(\bar{\xi}, \bar{\tau})$ firstly improves and then declines with increasing values of $(C_1), (Re)$ and (Pr).

Fig.12. (a- d) describes that the magnitude of Bejan number $(\overline{Be})$ decreases with (δ_1) and (Br), and it grows for growing values of $(C_1),(\alpha_2),(\alpha_1),(Nb),(Pr)$ and (Nt).

The outcomes of dissimilar variables like $(C_1),(Re),(M)$ and (S) on $\left(\overline{C}_{\overline{f}} \operatorname{Re}_{\overline{s}}^{1/2}\right)$ at time interval $\overline{\tau} \in (0,10\pi)$ are demonstrates through Fig.13. (a-d). This figure depicts that the amplitude of drag wall force coefficient is declined with (Re) and (M), whilst it is enlarged with amplifying values of (S) and (C_1).

Fig.14. (a-d) displayed the change in wall resistance force coefficient $\left(\operatorname{Re}_{\overline{s}}^{1/2} \overline{C}_{\overline{f}}\right)$ for various constants at $\overline{\tau} = 0.5\pi$. The influences of (C_1) versus (M) on $\left(\operatorname{Re}_{\overline{s}}^{1/2} \overline{C}_{\overline{f}}\right)$ can be seen in Fig.14. (a-b). The wall drag force magnitude is increased with (C_1), while it is declined with varying (M). Fig.14. (c-d) is made to shown the impacts of variable (S) vs (Re) on $\left(\operatorname{Re}_{\overline{s}}^{1/2} \overline{C}_{\overline{f}}\right)$. It can notice from this figure that the $\left(\operatorname{Re}_{\overline{s}}^{1/2} \overline{C}_{\overline{f}}\right)$ magnitude is reduced with uplifting (Re) and amplified with an enhancement in (S).

(a)

(b)

(c)

(d)
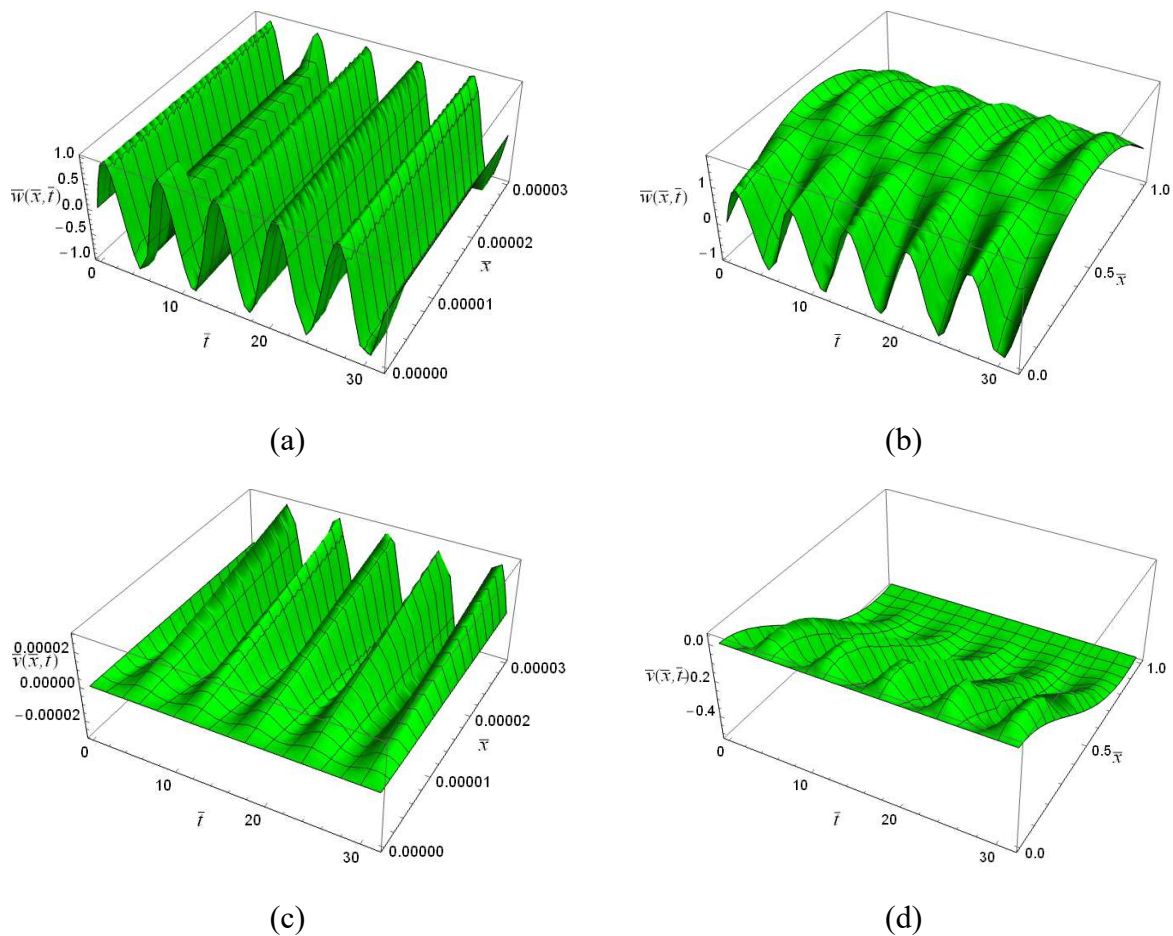
FIG. 2. 3- D view of axial components of velocity $\bar{u}(\bar{x},\bar{t})$ (a) for lower oscillatory curved wall (b) for upper porous wall; 3-D view of the normal components of velocity $\bar{v}(\bar{x},\bar{t})$ (c) for lower oscillatory curved wall (d) for upper porous wall. (For lower wall $\bar{x}=3\times10^{-5}$ and for upper wall $\bar{x}=1$).

(a) $\bar{t}\in(-0.5\pi,0.5\pi)$ (b) $\bar{t}\in(0,10\pi)$ (c) $\bar{t}\in(0,2\pi)$
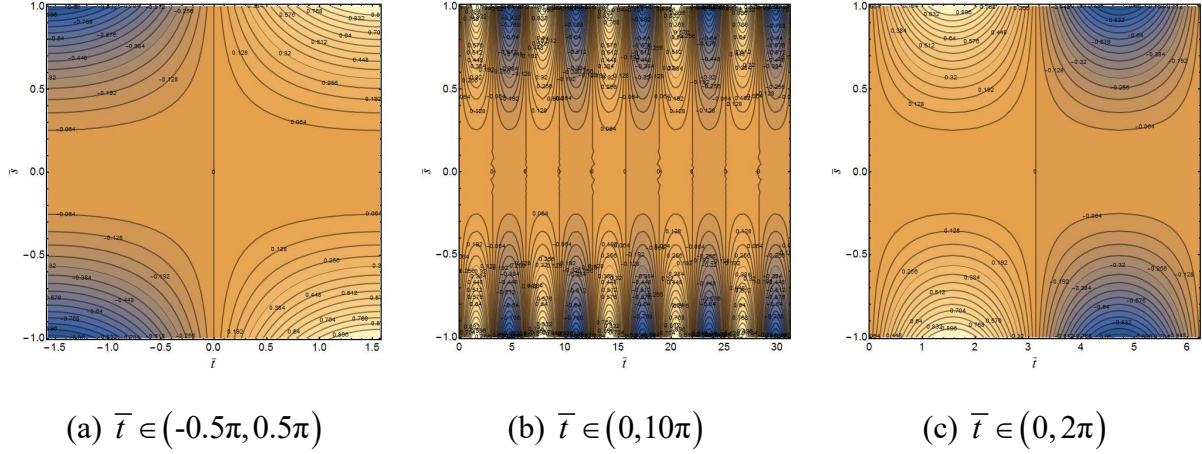
FIG.3. Variations in stream lines of $\bar{u}(\bar{x},\bar{t})$ by taking $\bar{x}\to0$ i.e. ($\bar{x}=3\times10^{-5}$) with $C_1=1.0, M=0.5, Re=0.5$ and $S=0.1$.

(a) $\bar{t}\in(-0.5\pi,0.5\pi)$ (b) $\bar{t}\in(0,10\pi)$ (c) $\bar{t}\in(0,2\pi)$
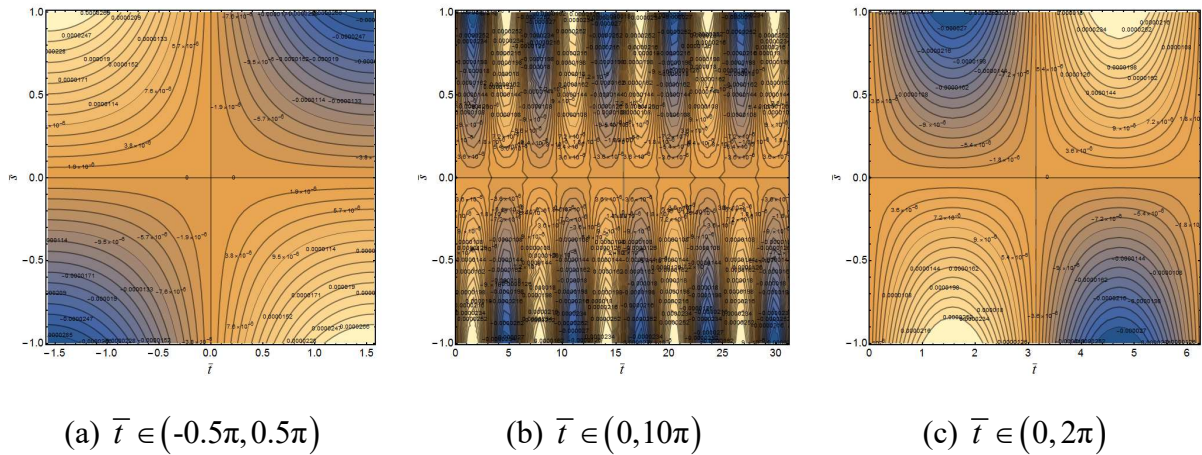
FIG.4. Variations in stream lines of $\bar{v}(\bar{x},\bar{t})$ by taking by taking $\bar{x}\to0$ i.e. ($\bar{x}=3\times10^{-5}$) with $S=0.1, M=0.5, Re=0.5$, and $C_1=1.0$.
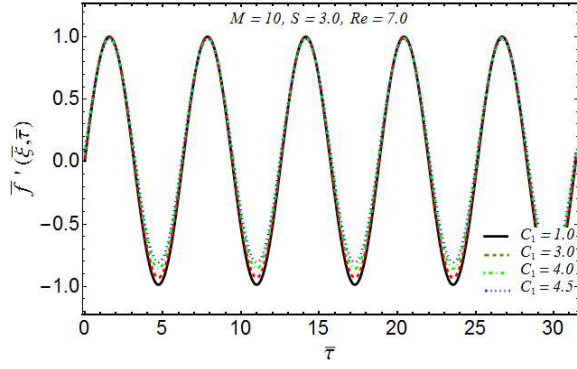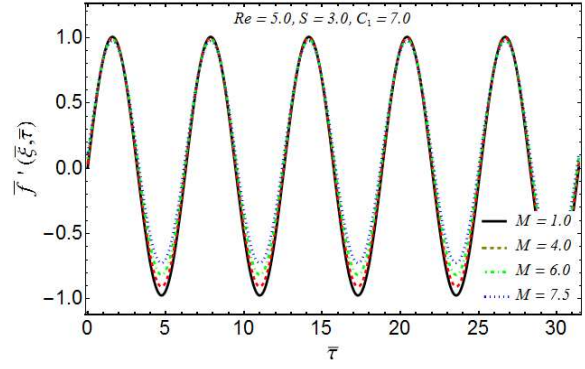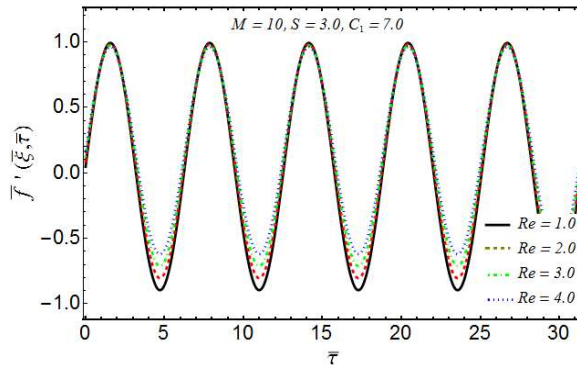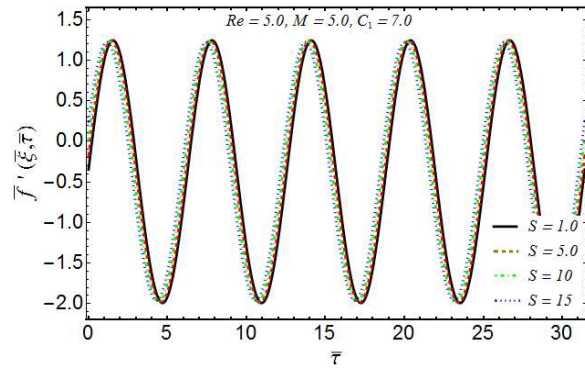
FIG.5. Variation of various fluid parameters on time series velocity field $\overline{f}'\left(\overline{\xi},\overline{\tau}\right)$ for the time interval $\overline{\tau} \in \left(0,10\pi\right)$ from the fixed distance to the surface (a) Impacts of C_1; (b) Impacts of M; (c) Impacts of Re; (d) Impacts of S by keeping other parameters fixed.
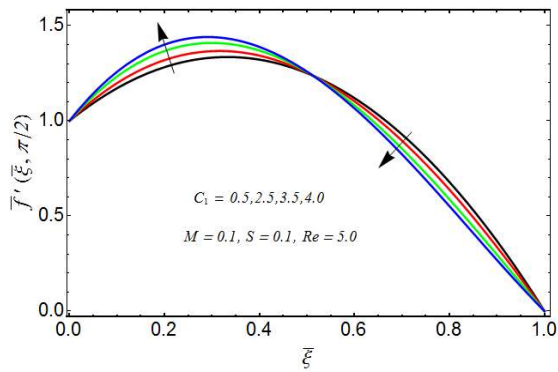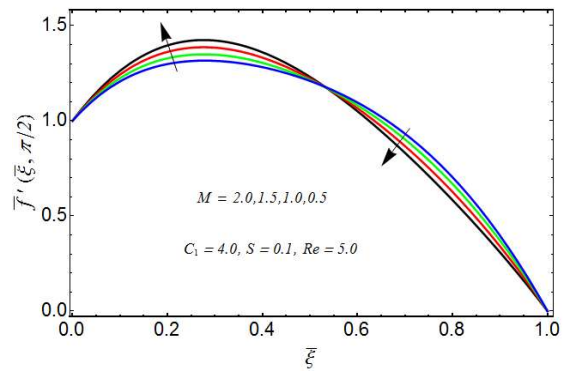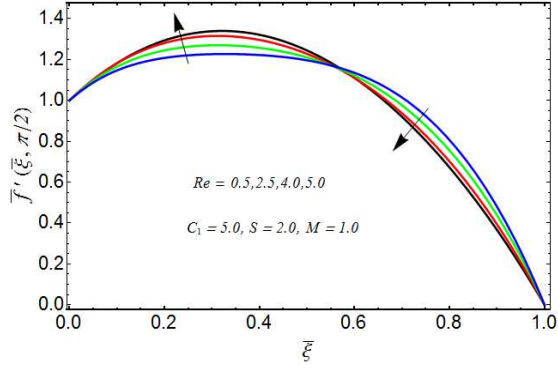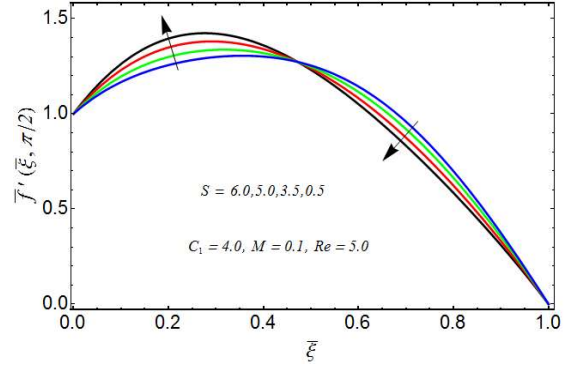
(c)   (d)

FIG.6. Variation of various fluid parameters on velocity field $\overline{f}'\left(\overline{\xi},\overline{\tau}\right)$ when $\overline{\tau}=0.5\pi$. (a) Impacts of C_1; (b) Impacts of M; (c) Impacts of Re; (d) Impacts of S by keeping other parameters fixed.
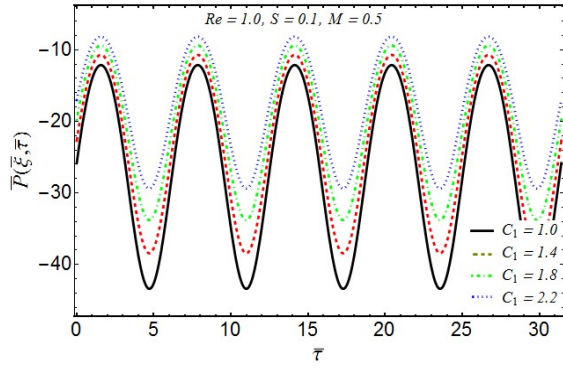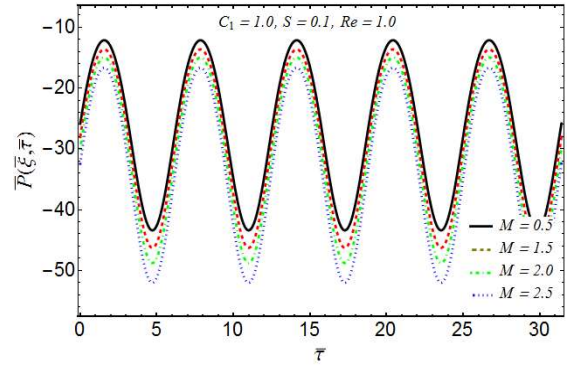
(a)   (b)
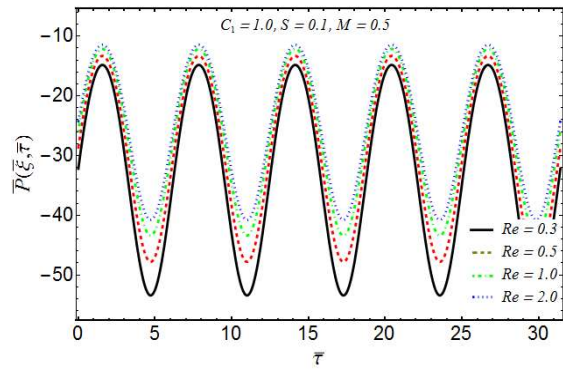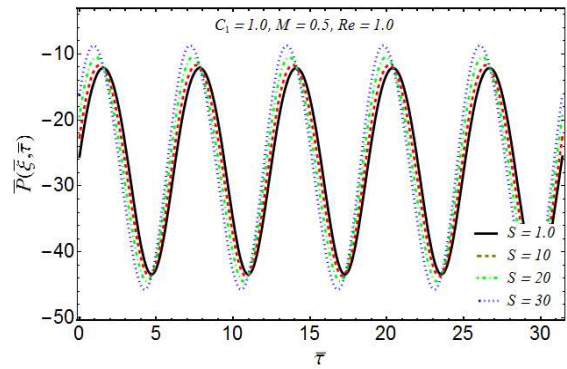
(c)   (d)

FIG.7. Variation of various fluid parameters on pressure profile $\overline{P}\left(\overline{\xi},\overline{\tau}\right)$ for the time interval $\overline{\tau}\in\left(0,10\pi\right)$ (a) Impacts of C_1; (b) Impacts of M; (c) Impacts of Re; (d) Impacts of S by keeping other parameters fixed.
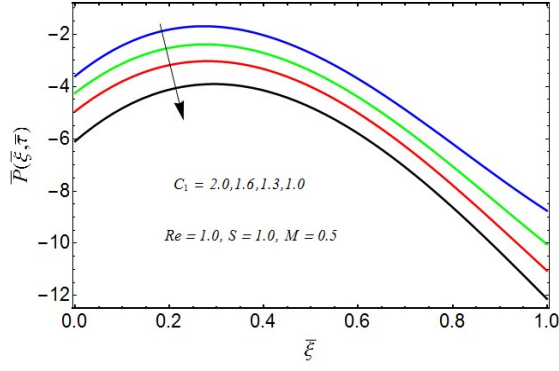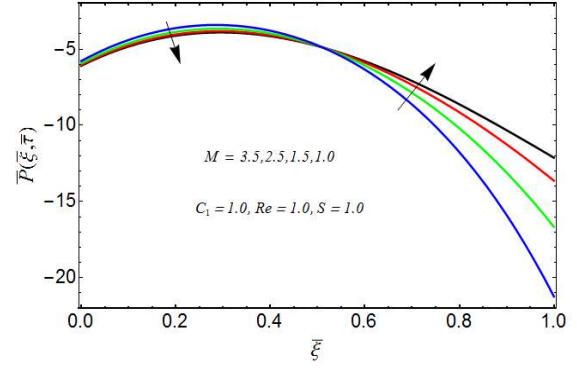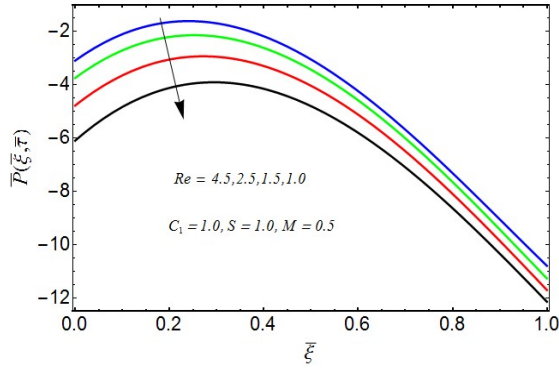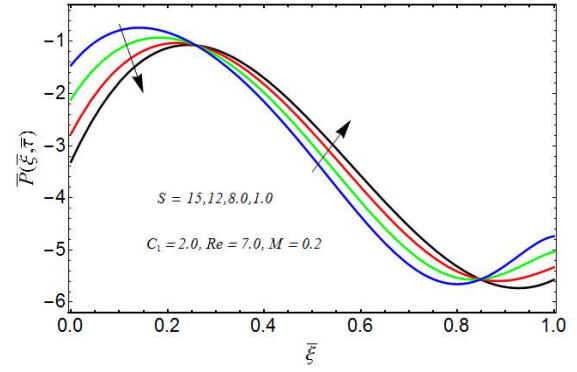
FIG.8. Variation of various fluid parameters on pressure profile $\overline{P}\left(\overline{\xi},\overline{\tau}\right)$ at $\overline{\tau} = 0.5\pi$. (a) Impacts of C_1; (b) Impacts of M; (c) Impacts of Re; (d) Impacts of S by keeping other parameters fixed.
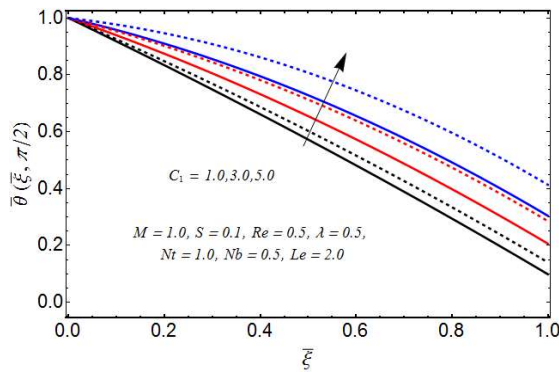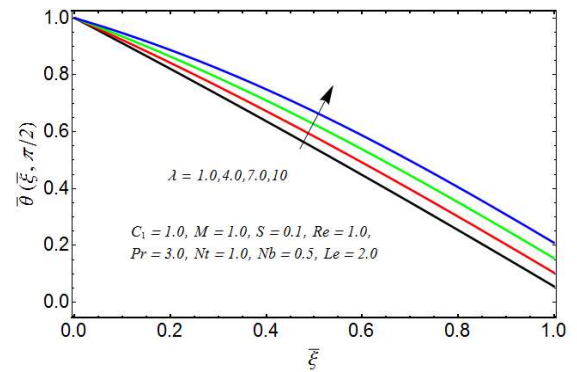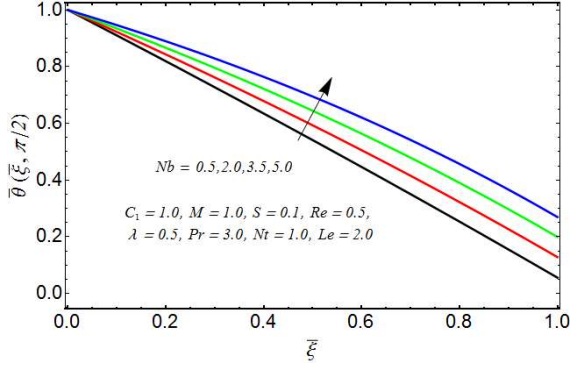
(c)
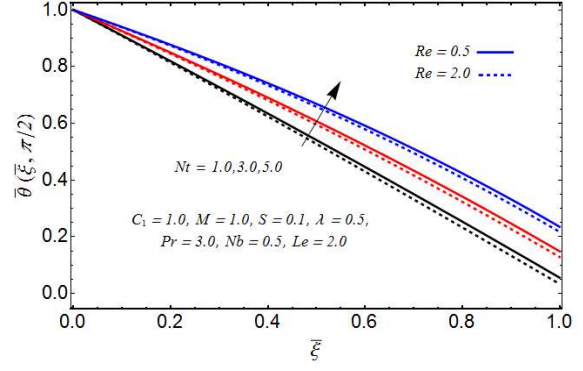
(d)

FIG.9. Variation of various flow parameters on temperature profile $\overline{\theta}\left(\overline{\xi},\overline{\tau}\right)$ for $\overline{\tau}=0.5\pi$. (a) Impacts of C_1 and Pr; (b) Impacts of λ; (c) Impacts of Nb; (d) Impacts of Nt and Re by keeping other parameters fixed.
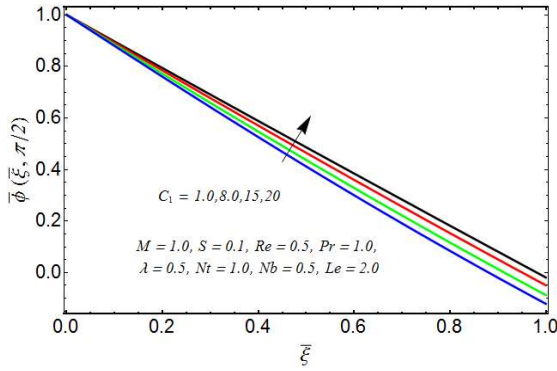
(a)
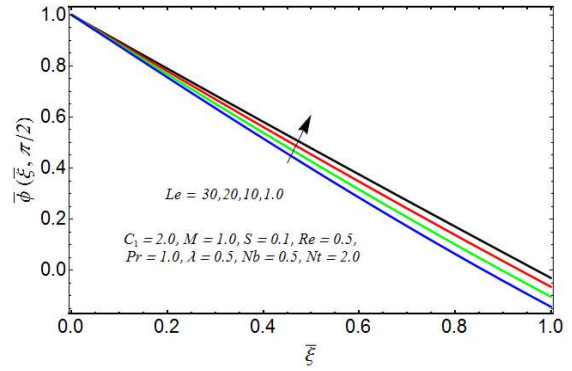
(b)
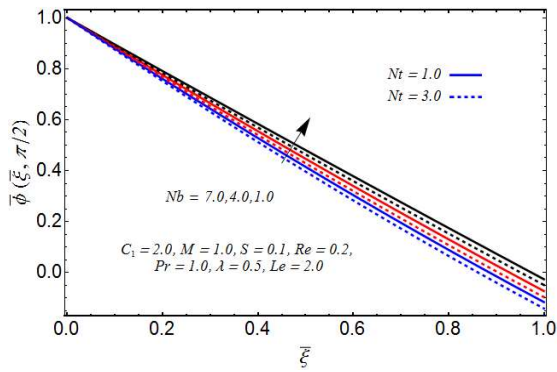
(c)
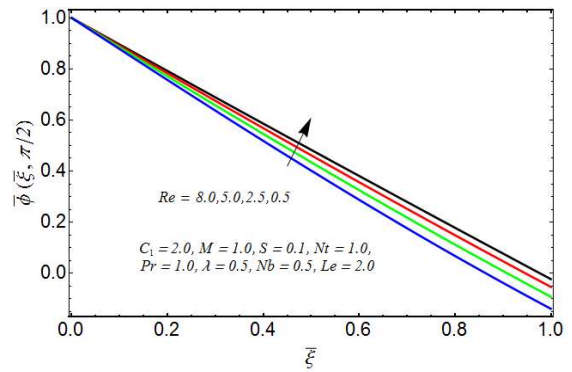
(d)

FIG.10. Variation of various flow parameters on concentration profile $\overline{\phi}\left(\overline{\xi},\overline{\tau}\right)$ for $\overline{\tau}=0.5\pi$. (a) Impacts of C_1; (b) Impacts of Le; (c) Impacts of Nb and Nt; (d) Impacts of Re by keeping

other parameters fixed.

(a)

(b)

(c)

(d)
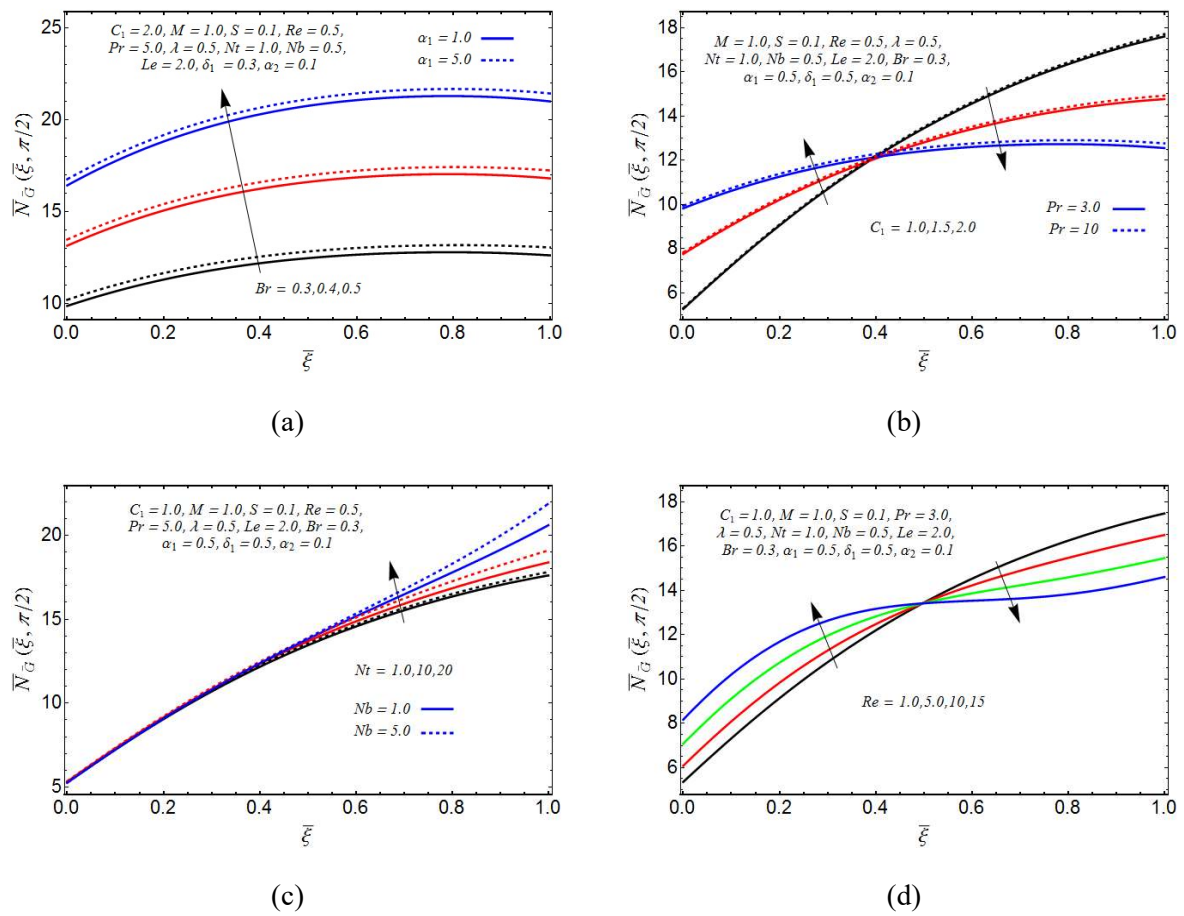
FIG.11. Variation of various flow parameters on entropy generation profile $\overline{N}_{\tilde{G}}\left(\overline{\xi}, \overline{\tau}\right)$ for $\overline{\tau} = 0.5\pi$. (a) Effects of α_1 and Br; (b) Impacts of C_1 and Pr; (b) Effects of Nt and Nb; (d) Impacts of Re by keeping other parameters fixed.

(a)

(b)
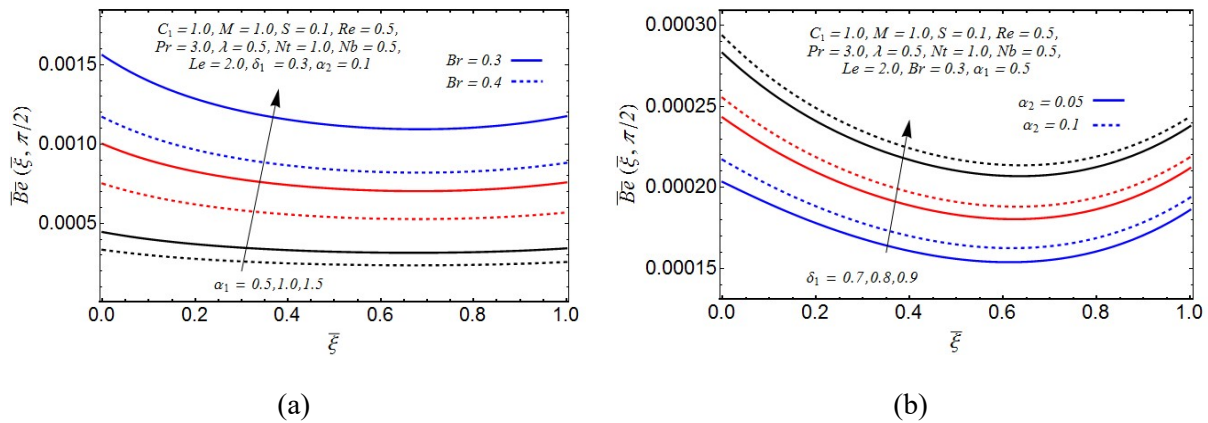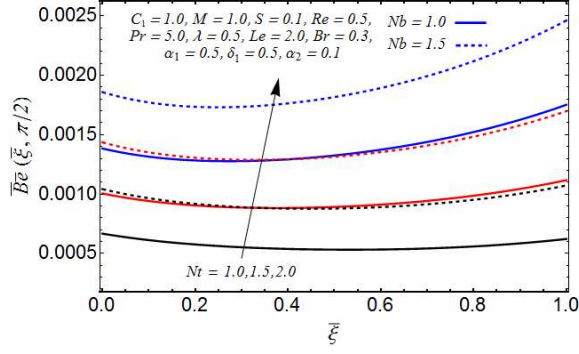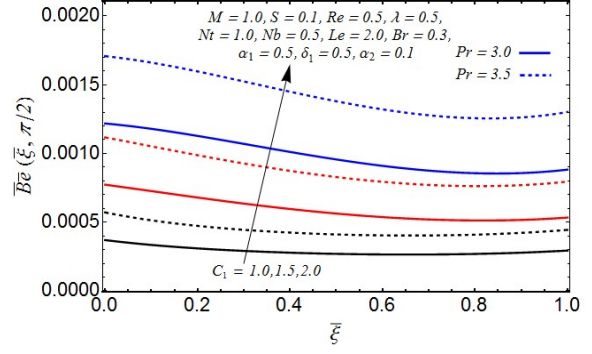
FIG.12. Variation of various flow parameters on Bejan number $\left(\overline{Be}\right)$ at $\overline{\tau}=0.5\pi$. (a) Effects of α_1 and Br; (b) Effects of α_2 and δ_1; (c) Impacts of Nt and Nb; (d) Impacts of C_1 and Pr by keeping other parameters fixed.
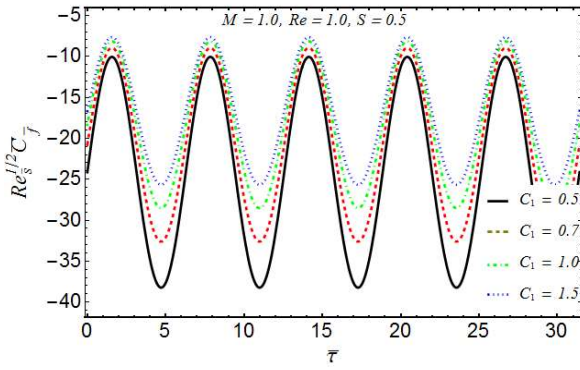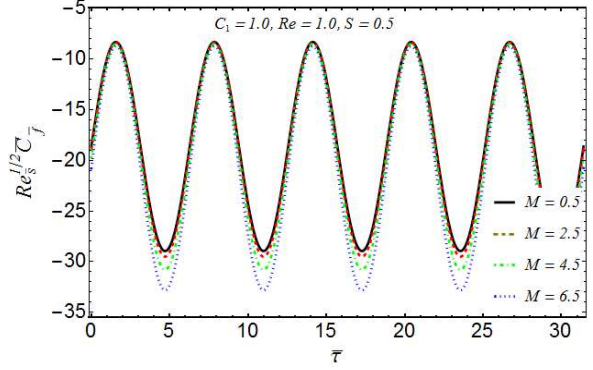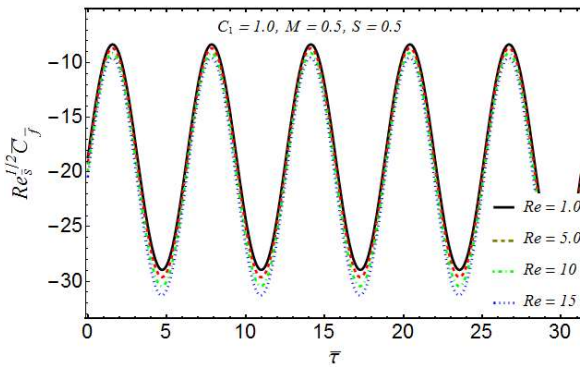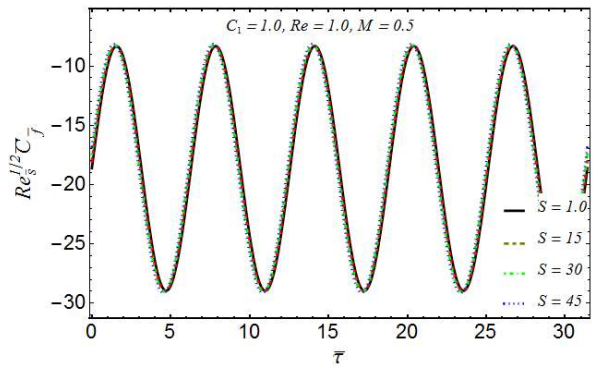
FIG.13. Variation of various flow parameters on time series for the surface drag force coefficient $\left(\operatorname{Re}_{\overline{s}}^{1/2}\overline{C}_{\overline{f}}\right)$ at $\overline{\tau}\in\left(0,10\pi\right)$. (a) Consequences of C_1; (b) Consequences of M; (c)

Consequences Re; (d) Consequences of S by keeping other parameters fixed.

(a)

(b)

(c)

(d)
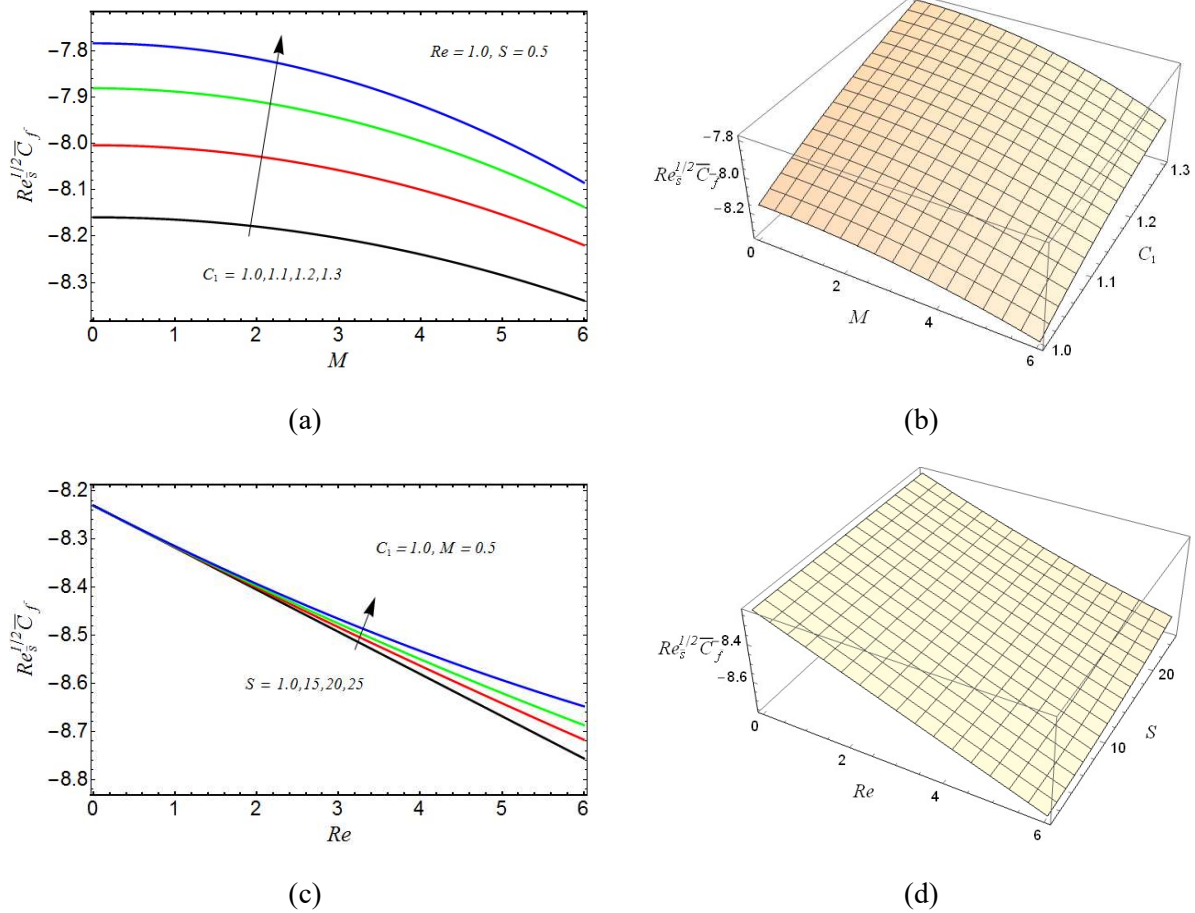
FIG.14. (a) Variations in $\left(\operatorname{Re}_{\overline{s}}^{1/2}\overline{C}_{\overline{f}}\right)$ with K_1 versus M; (b) 3- D view of variations in $\left(\operatorname{Re}_{\overline{s}}^{1/2}\overline{C}_{\overline{f}}\right)$ with C_1 versus M; (c) Variations in $\left(\operatorname{Re}_{\overline{s}}^{1/2}\overline{C}_{\overline{f}}\right)$ with S versus Re; (d) 3- D view of variations in $\left(\operatorname{Re}_{\overline{s}}^{1/2}\overline{C}_{\overline{f}}\right)$ with S versus Re when $\overline{\tau}=0.5\pi$.

Table 1: Numerical assessment of $\left(\overline{Nu}_{\overline{s}} \, \text{Re}_{\overline{s}}^{-1/2}\right)$ for some values of $(C_1), (Pr), (Re), (\lambda), (Nb)$ and (Nt) by using $M = 1.0, S = 0.1$ and $Le = 2.0$ fixed at $\overline{\tau} = 0.5\pi$.

C_1	Pr	Re	Nt	λ	Nb	$\left(\overline{Nu}_{\overline{s}} \, \text{Re}_{\overline{s}}^{-1/2}\right)$
1.0	1.0	0.5	0.5	0.5	0.3	0.998493
2.0						0.986005
3.0						0.973701
1.0	1.5					0.987841
	2.0					0.977223
	2.5					0.966638
	1.0	1.0				0.995181
		2.5				0.985223
		4.0				0.975232
		0.5	0.6			0.995520
			0.8			0.989588
			1.0			0.983673
			0.5	1.0		0.995181
				2.0		0.988546
				3.0		0.981896
				0.5	0.4	0.995509
					0.7	0.986555
					1.0	0.977600

Table 2: Assessment values of $\left(\bar{S}\,\bar{h}_{\bar{s}}\,\mathrm{Re}_{\bar{s}}^{-1/2}\right)$ for some unalike values of $(C_1),(Nt),(Re),(Pr),(Le)$ and (Nb) by using $M=1.0, S=0.1$ and $\lambda=0.5$ fixed at $\bar{\tau}=0.5\pi$.

C_1	Nt	Pr	Re	Nb	Le	$\left(\bar{S}\,\bar{h}_{\bar{s}}\,\mathrm{Re}_{\bar{s}}^{-1/2}\right)$
1.0	0.5	1.0	0.5	0.5	0.2	1.01515
3.0						1.01761
5.0						1.02030
1.0	0.6					1.01716
	0.7					1.01917
	0.8					1.02118
	0.5	2.0				1.01520
		6.0				1.01538
		10				1.01557
		1.0	1.0			1.01631
			2.0			1.01864
			3.0			1.02096
			0.5	0.3		1.01773
				0.4		1.02031
				0.5		1.02289
				0.2	1.5	1.01573
					3.0	1.01749
					4.5	1.01924

6. Conclusions

In this current study, we have investigated entropy production and the effects of heat production on viscous nanoliquid motion by considering Buongiorno's model in a semi-porous curved oscillating channel. The analytical outcomes of the governed nonlinear partial

differential flow equations are accomplished by implementing HAM. Consequences of unalike variables on concentration, velocity, temperature, Bejan number, skin friction coefficient, entropy production, local Nusselt number and on Sherwood number are established through tables and graphs and deliberated in details. The following specific conclusions are commented from present examination which are stated as

- The liquid velocity amplitude depicts declining response with growing values of $(C_1),(M)$ and (Re) for $\overline{\tau} \in (0,10\pi).$ Whilst, it improves with (S).

- The fluid velocity profile expresses increasing demeanor for improving (C_1) at $\overline{\tau} = 0.5\pi.$ However, it shows decaying response with $(Re),(M)$ and (S).

- For elevating values of $(C_1),(Re)$ and (S) the pressure distribution amplitude enlarges. While, it reduces with (M).

- At $\overline{\tau} = 0.5\pi$ the pressure distribution is declined with altering values of (S) and (M). However, profile of pressure field enhances for (C_1) and (Re).

- With improving values of $(C_1),(Nt),(\lambda),(Nb)$ and (Pr) the temperature of the liquid is enhanced. And, it diminishes with varying (Re).

- The concentration distribution displays reducing response with $(C_1),(Nt),(Le),(Pr),$ (Nb) and (λ).

- Entropy production profile shows mounting behavior with $(\alpha_1),(Nb),(Br)$ and (Nt).

- With (Br) and $(\delta_1),$ the Bejan number magnitude depicts decreasing manner. However, it enlarges for uplifting values of $(C_1),(\alpha_1),(Nt),(\alpha_2),(Pr)$ and (Nb).

- The drag surface force amplitude improves with (S) and (C_1). However, it decreases steadily for advanced values of (Re) and (M).

- The absolute values of rate of mass transmission is amplified with $(C_1),(Nt),(Re),(Nb),(Pr)$ and (Le).

- With uplifting $(C_1),(Pr),(Re),(Nb),(\lambda)$ and $(Nt),$ the magnitude of absolute values of heat transmission rate declines.

References

[1] A. S. Berman, Laminar flow in channels with porous walls. Journal of Applied physics 24.9(1953): 1232-1235.

[2] J. F. M . White, Laminar flow in a uniformly porous tube. (1962): 201-204.

[3] Z. Abbas, M. Sajid, and T. Hayat. MHD boundary-layer flow of an upper-convected Maxwell fluid in a porous channel. Theoretical and Computational Fluid Dynamics 20.4 (2006): 229-238.

[4] B. Raftari, F. Parvaneh, K. Vajravelu, Homotopy analysis of the magnetohydrodynamic flow and heat transfer of a second grade fluid in a porous channel. Energy 59 (2013): 625-632.

[5] N. Ali, S. U. Khan, M. Sajid, Z. Abbas, Flow and heat transfer of hydromagnetic Oldroyd-B fluid in a channel with stretching walls. Nonlinear Engineering 5.2(2016): 73-79.

[6] Z. Abbas, M. Naveed, M. Naeem, Q. M. Z. Zia. Analytical investigation of a Maxwell fluid flow with radiation in an axisymmetric semi-porous channel by parameterized perturbation method. Journal of the Brazilian Society of Mechanical Sciences and Engineering 40.2(2018): 65.

[7] M. Aleem, M. I. Asjad, A. Ahmadian, M. Salimi, M. Ferrara, Heat transfer analysis of channel flow of MHD Jeffrey fluid subject to generalized boundary conditions. The European Physical Journal Plus 135.1(2020): 1-15.

[8] S. A. Khuri, Stokes flow in curved channels. Journal of computational and applied mathematics 187.2(2006): 171-191.

[9] W.S. Fu, C. J. Chen, Y. C. Lai, S.H. Huang, Effects of a porous medium on forced convection of a reciprocating curved channel. International Communications in Heat and Mass Transfer 58 (2014): 63-70.

[10] Z. Abbas, M. Naveed, M. Sajid, Nonlinear radiative heat transfer and Hall effects on a viscous fluid in a semi-porous curved channel. AIP Advances 5.10(2015): 107124.

[11] M. Naveed, Z. Abbas, M. Sajid, Flow and heat transfer in a semiporous curved channel with radiation and porosity effects. Journal of Porous Media 19.5(2016).

[12] M. Sajid, S. A. Iqbal, M. Naveed, Z. Abbas. Joule heating and magnetohydrodynamic effects on ferrofluid (Fe3O4) flow in a semi-porous curved channel. Journal of Molecular Liquids 222 (2016): 1115-1120.

[13] Z. Abbas, M. Imran, M. Naveed, Hydromagnetic flow of a Carreau Fluid in a curved channel with non-linear thermal radiation, Thermal Science 00 (2018): 77-77.

[14] Z. Abbas, M. Rafiq, and M. Naveed. Analysis of Eyring–Powell liquid flow in curved channel with Cattaneo–Christov heat flux model. Journal of the Brazilian Society of Mechanical Sciences and Engineering 40.8(2018): 390.

[15] J. C. Misra, G. C. Shit, S. Chandra, P. K. Kundu, Hydromagnetic flow and heat transfer

of a second-grade viscoelastic fluid in a channel with oscillatory stretching walls: application to the dynamics of blood flow. Journal of Engineering Mathematics 69.1 (2011): 91-100.

[16] F. Ali, I. Khan, N. Mustapha, S. Shafie, Unsteady magnetohydrodynamic oscillatory flow of viscoelastic fluids in a porous channel with heat and mass transfer. Journal of the Physical Society of Japan 81.6(2012): 064402.

[17] A. Ali, S. Asghar, Analytic solution for oscillatory flow in a channel for Jeffrey fluid. Journal of Aerospace Engineering 27.3(2014): 644-651.

[18] S. U. Khan, N. Ali, M. Sajid, T. Hayat, Heat transfer characteristics in oscillatory hydromagnetic channel flow of Maxwell fluid using Cattaneo–Christov model. Proceedings of the National Academy of Sciences, India Section A: Physical Sciences 89.2(2019): 377-385.

[19] Z. Abbas, M. Imran, M. Naveed, Time-dependent flow of thermally developed viscous fluid over an oscillatory stretchable curved surface. Alexandria Engineering Journal (2020).

[20] M. Imran, Z. Abbas, M. Naveed, N. Salamat, Impact of Joule heating and melting on time-dependent flow of nanoparticles due to an oscillatory stretchable curved wall. Alexandria Engineering Journal 60.4 (2021): 4097-4113.

[21] S. U. S. Choi, Enhancing thermal conductivity of fluids with nanoparticle, In proceedings of the ASME International Mechanical Engineering Congress and Exposition 66 (1995) $99 - 105$.

[22] Buongiorno, J. (2006). Convective transport in nanofluids. Journal of Heat Transfer, 128, 240-250. Retrieved from https://doi.org/10.1115/ 1.2150834.

[23] M. Sheikholeslami, M. Hatami, D. D. Ganji, Analytical investigation of MHD nanofluid flow in a semi-porous channel. Powder Technology 246 (2013): 327-336.

[24] M. Naveed, Z. Abbas, and M. Sajid, Thermophoresis and Brownian effects on the Blasius flow of a nanofluid due to a curved surface with thermal radiation. The European Physical Journal Plus 131.6 (2016): 214.

[25] A. Alblawi, M. Y. Malik, S. Nadeem, N. Abbas, Buongiorno's Nanofluid Model over a Curved Exponentially Stretching Surface. Processes 7(10) (2019): 665.

[26] Z. Z. Rashed, S. E. Ahmed, Peristaltic flow of dusty nanofluids in curved channel. CMC-COMPUTERS MATERIALS & CONTINUA 66.1(2021): 1011-1026.

[27] A. Riaz, S. U. D. Khan, A. Zeeshan, S. U. Khan, M. Hassan, T. Muhammad, Thermal analysis of peristaltic flow of nanosized particles within a curved channel with second-order partial slip and porous medium. Journal of Thermal Analysis and Calorimetry (2020): 1-13.